THE AMERICAN SOCIETY OF MECHANICAL ENGINEERS
345 E. 47th St., New York, N.Y. 10017

96-TA-15

MODELING AND SIMULATION OF TRANSVERSE CRACKS FOR ROTOR-BEARING SYSTEMS

Tachung Yang **Shi-An Chen**

Department of Mechanical Engineering
Yuan Ze Institute of Technology
Taoyuan, Taiwan, ROC

ABSTRACT

Undetected cracking of rotating shafts can lead to catastrophic failure of turbomachinery. This paper investigated the dynamic response of rotor-bearing systems containing transverse cracks with a finite element approach. The breathing effect of cracks was analyzed based on the whirling conditions of the rotor, and different crack models were posed for different rotating speeds. The strain energy released due to the cracks was calculated. Then, the finite element for the shaft portion containing cracks was formulated and incorporated into the system matrices of the rotor-bearing system.

NOMENCLATURE

A:	crack area open at that instance
d:	Crack depth ratio, $=\alpha / R$
$\overline{E}$:	$=E$, Young's modulus, for plain stress
	$=E/(1-\nu^2)$, for plain strain
ν:	Poisson's ratio
G:	Shear modulus
I_{xx}, I_{yy}:	Transverse moment of inertia based on the crack area open
R:	Radius of the shaft
s^*:	Local coordinate of the crack
U_s:	Potential energy of the uncracked shaft
U_c:	Crack released energy
α:	Depth of crack
γ':	Inclined angle of the neutral axis
θ':	Whirling (or orbiting) angle of the shaft
ϕ:	Rotating angle of the shaft, $=\omega t$
ω:	Rotating frequency of the shaft
ϖ:	Rotating frequency of the neutral axis
Ω:	Whirling frequency of the shaft
$\bar{v}_d$:	Dynamic deflection
$\bar{v}_{st}$:	Static deflection
λ:	Deflection ratio$= v_d / v_{st}$

INTRODUCTION

If the shafts of rotating machinery contain cracks, the cracks grow as the machines continuously operate and may cause total machine failure and huge economic losses. When compared with the vibrating behavior of a flawless rotating shaft, abnormal vibrating behavior occurs for a cracked rotating shaft during operation. Since the crack effects on the shaft vibration are very complicated, modeling and simulation of the crack behavior during machinery operation to gain better understanding to the crack influence on the machine vibration is the objective of this study.

Major research advance on cracked shafts has begun since mid 1970 and can be roughly divided into two categories: (1) modeling of crack and (2) crack detection. See Wauer (1990) for an excellent review of the literature. Gasch (1976) modeled the transverse crack as a hinge, which contains the breathing effect of the crack. Grabowski (1980) utilized the inertia change of the cross section of the shaft to derive a linear time-variant equation of motion. Mayes and Davis (1984) obtained the flexibility caused by the crack using the Green function approach and found that a small crack can be replaced by a slot on the shaft. Papadopoulos and Dimarogonas (1988, 1992), and Dimarogonas and Paipetis (1983) applied principles of fracture mechanics to calculate the properties of a crack and generated a 6x6 flexibility matrix for the transverse crack effects. Nelson and Nataraj (1986) considered the stiffness change as a time variant function of the local bending curvature of the shaft, and introduced a switch function to simulate the crack breathing effects.

This study is to establish a more realistic crack model. The crack model considered in this study operated under gravitation and included the shear deformation effect, but did not include the internal damping, torsion and axial thrust effects. The crack effects were taken into account by the released energy approach and the Lagrange formulation was used to derived the stiffness-reduction term which represents the crack effects "globally". The stiffness reduction term was directly added to the equations of motion of the uncracked rotor-bearing systems.

MAJOR ASSUMPTIONS

Since the extension of a crack causes the strain energy to decrease in the neighborhood of the crack (Tada, 1985; Dimarogonas and Paipetis, 1983), it was assumed that the crack effects on the vibration response of the rotor-bearing system can be adequately represented by the crack released energy U_c. If the total potential energy of the uncracked rotor-bearing system is U_s, then $U_s - U_c$ is the total potential energy for the rotor-bearing system containing the crack. Since the cracked rotor-bearing system should still behave as a continuous system (C^1 continuous) and the vibration response of the shaft is analyzed from the global scale (not to emphasize on the accuracy of the local vibration responses near the crack), the finite element derivation of the equation of motion for a cracked rotor-bearing

Presented at the 1996 ASME Turbo Asia Conference
November 5-7, 1996 Jakarta, Indonesia

system should be similar to that of the general uncracked rotor-bearing system. The same shape functions and derivation procedure for the uncracked shaft can be used for the cracked shaft. At the expense of scarifying the response details at the exact crack location, the merit of the FEM approach is preserved by adding the stiffness-reduction term to the system stiffness matrix directly without the inverse of flexibility matrix. Multiple cracks located at different shaft elements can be handled easily in this way. The other hypothesis that we assumed is that the cracked shaft element should be at least twice as long as the crack depth, since the length of the influential zone of stiffness change due to the crack existence is about twice that of the crack depth (Grabowski, 1980).

CRACK MODELS AND BREATHING PROCESS

For a shaft with a transverse crack under the gravity effect (Fig. 1), the crack opens and closes alternatively as the shaft rotates. This periodic open-close behavior is called breathing. we can view the breathing as caused by the crack area (or the crack front) entering or exiting the compression zone through the neutral axis of the cross section of the shaft. Furthermore, we can say that the breathing behavior is determined by the relationship between the locations of the neutral axis and the crack front. The orientation of the crack front is determined by the shaft rotating (or spinning) angle, whereas the orientation of the neutral axis is determined by the deflection condition of the shaft. The shaft deflection consists of the static deflection $\bar{v}_{st}$ and the dynamic deflection $\bar{v}_d$. The geometrical relationship between these deflections and the neutral axis n-n can be shown in Fig. 2. Assuming the shaft rotates at a constant speed, and whirls synchronously, then,

$$\sin\gamma' = \frac{\|\bar{v}_d\|\cos\theta'}{\|\bar{v}_{st}+\bar{v}_d\|} \tag{1}$$

let $\|\bar{v}_d\| = v_d$, $\|\bar{v}_{st}\| = v_{st}$, we can obtain

$$\begin{aligned}\sin\gamma' &= \frac{v_d\cos\theta'}{\|(-v_{st}+v_d\sin\theta')\bar{j}+v_d\cos\theta'\,\bar{i}\|} \\ &= \frac{\cos\theta'}{[(\frac{v_{st}}{v_d})^2-2(\frac{v_{st}}{v_d})\sin\theta'+1]^{1/2}} \\ &= \frac{\cos\theta'}{[(\frac{1}{\lambda})^2-2(\frac{1}{\lambda})\sin\theta'+1]^{1/2}}\end{aligned} \tag{2}$$

$$\text{If } \lambda = 1, \text{ then } \sin\gamma' = \frac{\cos\theta'}{\sqrt{2}(-\sin\theta'+1)^{1/2}} \tag{3}$$

(a) If $v_d << v_{st}$ $(\lambda \to 0)$, $\sin\gamma' \cong 0$, $\gamma' = 0°$, from Eq. (2). γ' is independent of time, so the orientation of the neutral axis n-n is fixed, not affected by the spinning of the shaft. The crack area passes through the neutral axis periodically and creates periodic breathing.

(b) If $v_{st} << v_d$ $(\lambda \to \infty)$, then from Eq. (2), $\sin\gamma' \cong \cos\theta'$ $\gamma' = 90° + \theta'$, so $\varpi = \Omega = \omega$. The neutral axis n-n rotates at constant angular speed, $\varpi = \omega$, at steady condition, and is always perpendicular to the v_d directions, i.e. tangential to the whirling orbit of the shaft. The crack front is fixed with respect to the neutral axis as viewed from the rotating coordinate system. The crack may be fully open, fully closed, or partially open, depending on the initial conditions.

(c) If $v_{st} > v_d$ $(0 < \lambda < 1)$, then from Eq.(2), γ' varies periodically and the neutral axis n-n is in a see-saw motion. As v_d approaches v_{st} $(\lambda \to 1)$, variation of γ' becomes larger. At this time, the total crack area is under the breathing process.

(d) If $v_{st} < v_d$ $(1 < \lambda < \infty)$, then from Eq. (2), the neutral axis n-n rotates at a non-constant rate. As v_d approaches v_{st} ($\lambda \to 1$), the non-breathing situation ($\lambda \to \infty$) mentioned above, becomes breathing of the partial crack area for deep cracks, and no breathing for small cracks, depending on the crack depth and the initial conditions.

(e) If $v_{st} = v_d$ ($\lambda = 1$), total crack area breathes, but from Eq. (3), when $\theta' = 90°$, γ' does not exist, i.e., no neutral axis exists.

Summarized the above discussions, the following five crack breathing models can be established:

(1) Total crack (area) breathing
(2) Partial crack (area) breathing
(3) Partial crack (area) open, no breathing
(4) Full crack (area) open, no breathing
(5) Totally closed crack (area)

Models 4 and 5 are the special cases of model 3.

The conditions for these models to apply is as follows:

(1) when the vibration amplitude or the whirling orbit is small, like at the outset of the shaft startup, model 1 can be used.
(2) when the vibration amplitude is large or the shaft rotating speed is close to the critical speeds, one of models 2 through 5 can occur.

As the rotating speed of the shaft increases, the sequence of the breathing models is stationary-(1)-(2)-(3)-(4)-(5)-critical speed.

CRACK RELEASED ENERGY

Considering a shaft element containing a crack and its loading conditions, p_1, p_2 are the shear forces in x and y directions of the rotating coordinate system at the crack location, as shown in Fig. 3. p_3, p_4 are the bending moment, likewise. When the crack opens, the strain energy released (Tada, 1985; Dimarogonas and Paipetis, 1983) is

$$U_c = \int_A J dA \quad \text{or} \quad U_c = \int_A J(\alpha) d\alpha dx \tag{4}$$

$$\text{and } J(\alpha) = \frac{1}{E}[(\sum_{j=1}^{4} K_{Ij})^2 + (\sum_{j=1}^{4} K_{IIj})^2 + (1+\nu)(\sum_{j=1}^{4} K_{IIIj})^2] \tag{5}$$

where

K_{ij}: Stress Intensity Factors, SIF

$i = I, II, III$ fracture mode index

$j = 1,2,3,4$ loading index

$K_{I3} = \sigma_3\sqrt{\pi a}F_2(a/h)$ $\quad \sigma_3 = (4P_3/\pi R^4)(R^2 - x^2)^{1/2}$

$K_{I4} = \sigma_4\sqrt{\pi a}F_1(a/h)$ $\quad \sigma_4 = (4P_4/\pi R^4)x$

$K_{I1} = K_{I2} = 0$

$K_{II2} = \sigma_2\sqrt{\pi a}F_{II}(a/h)$ $\quad \sigma_2 = kP_2/(\pi R^2)$

$K_{II1} = K_{II3} = K_{II4} = 0$

$K_{III1} = \sigma_1\sqrt{\pi a}F_{III}(a/h)$ $\quad \sigma_1 = kP_1/(\pi R^2)$

$K_{III2} = K_{III3} = K_{III4} = 0$

$F_1(a/h) = (\tan\bar{\lambda}/\bar{\lambda})^2[0.752 + 2.02(a/h) + 0.37(1 - \sin\bar{\lambda})^3]/\cos\bar{\lambda}$

$F_2(a/h) = (\tan\bar{\lambda}/\bar{\lambda})^2[0.923 + 0.199(1 - \sin\bar{\lambda})^4]/\cos\bar{\lambda}$

$F_{II}(a/h) = [1.22 - 0.562(a/h) + 0.085(a/h)^2 + 0.18(a/h)^3]/(1 - a/h)^{1/2}$

$F_{III}(a/h) = (\tan\bar{\lambda}/\bar{\lambda})^{1/2}$

$\bar{\lambda} = \pi a/(2h)$ $\quad h = 2\sqrt{R^2 - x^2}$

$k = 6(1+\nu)/(7+6\nu)$

When the crack opens, the neutral axis does not pass through the center of the cross section of the shaft, but it passes through the centroid of the connected area of the shaft, where the centroid moves as the crack breathes. The parallel shift of the neutral axis was neglected in our analysis.

As shown in Fig. 4, the integration in Eq. (4) is calculated over the actual open area of the crack. Since the crack front and the neutral axis are not perpendicular to each other and the integration area varies as time changes, the integration area is simplified by integrating from the end point of the crack to the point p, where p is the intersection of the crack front, and the line L, which is found from the mid point of line segment $\overline{rs}$.

FINITE ELEMENT FORMULATION FOR CRACKS

From Eqs. (4) and (5), we obtain

$$U_c = \int_A J(\alpha)d\alpha dx\Big|_{s=s^*}$$

$$= \int_A \frac{\pi a}{\bar{E}}\left[\frac{16P_3^2}{(\pi R^4)^2}(R^2 - x^2)F_2^2 + \frac{16P_4^2}{(\pi R^4)^2}x^2F_1^2 + \frac{32P_3P_4}{(\pi R^4)^2}x(R^2 - x^2)^{1/2}F_1F_2\right.$$

$$\left. + \frac{k^2P_2^2}{(\pi R^2)^2}F_{II}^2 + \bar{m}\frac{k^2P_1^2}{(\pi R^2)^2}F_{III}^2\right]d\alpha dx\Big|_{s=s^*} \quad (6)$$

$P_1 = kA^*G\nu_s'$; $P_2 = kA^*Gw_s'$; $P_3 = -\bar{E}I_{xx}w''$; $P_4 = \bar{E}I_{yy}\nu''$ (7)

where I_{xx} and I_{yy} are the area moment of inertia for the connected area A^* of the shaft at the crack location, with respect to the rotating coordinate system. The connected area at the crack location is not symmetric, and changes periodically due to the crack breathing. So usually $I_{xx} \neq I_{yy}$, and values of I_{xx}, and I_{yy} are changed periodically.

Substituting Eq. (7), into Eq. (6), and we get

$$U_c\Big|_{s=s^*} = \int_A \frac{\pi a}{\bar{E}}\left[\frac{16(R^2 - x^2)F_2^2}{(\pi R^4)^2}(-\bar{E}I_{xx}w'')^2\right.$$

$$+ \frac{16x^2F_1^2}{(\pi R^4)^2}(\bar{E}I_{yy}\nu'')^2 - \frac{32x(R^2 - x^2)^{1/2}F_1F_2}{(\pi R^4)^2}\bar{E}^2I_{xx}I_{yy}w''\nu''$$

$$\left. + \frac{k^2F_{II}^2}{(\pi R^2)^2}(kA^*Gw_s')^2 + \frac{\bar{m}k^2F_{III}^2}{(\pi R^2)^2}(kA^*G\nu_s')^2\right]d\alpha dx\Big|_{s=s^*}$$

$$= U_{P_3^2} + U_{P_4^2} - U_{P_3P_4} + U_{P_2^2} + U_{P_1^2}$$

$$= \begin{Bmatrix} v \\ w \end{Bmatrix}^{*T}\begin{bmatrix} D_{11} & 0 \\ 0 & D_{22} \end{bmatrix}\begin{Bmatrix} v \\ w \end{Bmatrix}'' - cw''\nu'' + \begin{Bmatrix} v_s \\ w_s \end{Bmatrix}^{'T}\begin{bmatrix} B_{11} & 0 \\ 0 & B_{22} \end{bmatrix}\begin{Bmatrix} v_s \\ w_s \end{Bmatrix}'\Big|_{s=s^*} \quad (8)$$

where $U_{P_1^2}$ is the crack released energy due to p_1 loading, and $U_{P_3P_4}$ is the crack released energy due to the coupling of p_3 and p_4, etc.. The above (v,w), (v_s,w_s) are with respect to the rotating coordinate system. So they have to be transformed to the fixed coordinate system, (V,W), (V_s,W_s) in $\Im XYZ$.

$$\begin{Bmatrix} v \\ w \end{Bmatrix} = [R]^T\begin{Bmatrix} V \\ W \end{Bmatrix}\ ;\ \begin{Bmatrix} v_s \\ w_s \end{Bmatrix} = [R]^T\begin{Bmatrix} V_s \\ W_s \end{Bmatrix}\ ;\ [R] = \begin{bmatrix} \cos\phi & -\sin\phi \\ \sin\phi & \cos\phi \end{bmatrix} \quad (9)$$

converting the displacements $V(s,t)$, $W(s,t)$, $V_s(s,t)$, $W_s(s,t)$ into nodal displacements, we obtain

$$\begin{Bmatrix} V(s,t) \\ W(s,t) \end{Bmatrix} = \{\varphi(s)\}\{q^s(t)\} = \begin{Bmatrix} \varphi_V \\ \varphi_W \end{Bmatrix}\{q^s(t)\} \quad (10)$$

$$\begin{bmatrix} \varphi_V \\ \varphi_W \end{bmatrix} = \frac{1}{1+\Phi}\begin{bmatrix} \xi_1 & 0 & 0 & \xi_2 & \xi_3 & 0 & 0 & \xi_4 \\ 0 & \xi_1 & -\xi_2 & 0 & 0 & \xi_3 & -\xi_4 & 0 \end{bmatrix}$$

$$\begin{Bmatrix} V_s(s,t) \\ W_s(s,t) \end{Bmatrix} = \frac{\Phi}{1+\Phi}\begin{Bmatrix} \bar{\varphi}_V \\ \bar{\varphi}_W \end{Bmatrix}_s\{q^s(t)\} = \{\varphi(s)\}_s\{q^s(t)\} \quad (11)$$

$$\begin{Bmatrix} \bar{\varphi}_v \\ \bar{\varphi}_w \end{Bmatrix}_s = \begin{Bmatrix} 1-\varepsilon & 0 & 0 & \frac{l}{2}(\varepsilon - \varepsilon^2) & \varepsilon & 0 & 0 & \frac{l}{2}(-\varepsilon + \varepsilon^2) \\ 0 & 1-\varepsilon & -\frac{l}{2}(\varepsilon - \varepsilon^2) & 0 & 0 & \varepsilon & -\frac{l}{2}(-\varepsilon + \varepsilon^2) & 0 \end{Bmatrix}$$

where ξ_i is the shape function, $\varepsilon = \frac{s}{l}$, and $\{q^s(t)\}_{8\times1}$ is the nodal displacement vector of the cracked shaft element. In Eqs. (10) and (11), $\Phi = \frac{12\bar{E}I_{yy}}{kA^*Gl^2}$ is used to calculate $v(s,t)$ and $v_s(s,t)$, and $\Phi = \frac{12\bar{E}I_{xx}}{kA^*Gl^2}$ is used to calculate $w(s,t)$ and $w_s(s,t)$.

Substituting Eqs. (9)(10)(11) into Eq. (8), and putting U_c into Lagrange formulation,

$$\left.\frac{\partial U_e}{\partial q(t)}\right|_{s=s^*} = \{2\{\varphi\}''^T[R][D][R]^T\{\varphi\}'' + 2\{\varphi\}_s'^T[R][B][R]^T\{\varphi\}_s'$$

$$-2c\left\{\{\varphi_V\}\cos\phi+\{\varphi_W\}\sin\phi\right\}''^T\left\{-\{\varphi_V\}\sin\phi+\{\varphi_W\}\cos\phi\right\}''\}\left\{q^s(t)\right\}$$

$$=-([Z_0]+[Z_c]\cos 2\phi+[Z_s]\sin 2\phi)\left\{q^s(t)\right\}=[K_c]\left\{q^s(t)\right\} \quad (12)$$

where

$$[R][D][R]^T=\frac{1}{2}\begin{bmatrix}(D_{11}-D_{22})\cos 2\phi+(D_{11}+D_{22}) & (D_{11}-D_{22})\sin 2\phi\\ (D_{11}-D_{22})\sin 2\phi & (D_{22}-D_{11})\cos 2\phi+(D_{11}+D_{22})\end{bmatrix}$$

$$[R][B][R]^T=\frac{1}{2}\begin{bmatrix}(B_{11}-B_{22})\cos 2\phi+(B_{11}+B_{22}) & (B_{11}-B_{22})\sin 2\phi\\ (B_{11}-B_{22})\sin 2\phi & (B_{22}-B_{11})\cos 2\phi+(B_{11}+B_{22})\end{bmatrix}$$

The $[K_c]$ term is the stiffness-reduction term for the crack as mentioned in the introduction. Adding the $[K_c]$ term directly to the system stiffness matrix, similar to the usual finite element procedure, the global system equation of motion becomes

$$[M]\left\{\ddot{q}^s\right\}+[C]\left\{\dot{q}^s\right\}+([K]-[K_c])\left\{q^s\right\}=\left\{Q^s\right\} \quad (13)$$

In Eq. (13), the $[M]$, $[C]$, $[K]$ terms are constant matrices and are derived from the uncracked rotor-bearing system. The $[Z_0]$, $[Z_c]$, $[Z_s]$ terms are not always constant matrices, depending on the crack breathing models used. When crack breathing models 1 or 2 is used, Eq. (13) becomes a nonlinear equation with time variant coefficients. When crack breathing models 3 or 4 is used, Eq. (13) becomes a linear equation with time variant coefficients. If model 5 is used, $[K_c]$ disappears, and Eq. (13) is reduced to a linear equation with constant coefficients, as the usual rotordynamic equation for the uncracked rotor-bearing systems.

Harmonic balance method (Nelson, and Nataraj, 1986) is used to solve the vibration responses from Eq. (13).

NUMERICAL RESULTS

The rotor-bearing system for the subsequent analysis is shown in Fig. 1, and its dimensions and properties is shown in Table 1 . The crack released energy for the shaft element with a crack at its mid-span can be calculated from Eq. (6) for p_1, p_2, p_3, and p_4 separately. Figures 5, 6, and 7 show the crack released energy, $U_{p_1^2}$, $U_{p_3^2}$, $U_{p_3p_4}$, of breathing model 1 for each loading condition in the rotating coordinate system, in which $v_s'=w_s'=w''=v''=1$ for the comparison purpose. The normal direction of the crack front and the negative Y direction of the fixed reference frame coincide when t=0.

The horizontal portions of the curve, d=0.6 in $U_{p_1^2}$ of Fig. 5, reach maximum during the intervals of $0^\circ\sim 50^\circ$ and $310^\circ\sim 360^\circ$, which means the crack is in fully open, while $U_{p_1^2}$=0 during $130^\circ\sim 230^\circ$ means the crack is fully closed. The other portions of the curve show the crack is under breathing and the energy releasing process is continuous and smooth. The curve of $U_{p_3p_4}$ in Fig. 7 is due to the coupling effects of the bending moments, p_3 and p_4. The coupling effects disappear when the crack is fully closed or fully open, and the coupling effects reach maximum values when the shaft rotates to 90° and 270°.

Also note that the crack released energy $U_{p_3^2}$ in Fig. 6, is about $600\sim 1500$ times of the crack released energy $U_{p_1^2}$ in Fig. 5. This means that even for the crack, the effects of bending moments are dominant over the effects of shear forces for slender shafts. Therefore, the shear deformation effects can be neglected in the cases of slender shafts.

The stiffness reduction term $[K_c]_{8\times 8}$ consists of 64 components for the cracked shaft element 3 of the rotor-bearing system (Fig. 1). The values of the K_{11}^c, K_{22}^c, K_{33}^c, and K_{44}^c, relative to the fixed reference frame are shown in Figs. 8-11. K_{11}^c and K_{22}^c have the maximum values when the crack is fully open, and become zero when the crack is fully closed.

Figure 12 and 13 are the 1/rev and 2/rev responses of the cracked rotor-bearing system with the crack depth ratio $d=0.4$ and model 1 is used for the crack breathing. The static deflection line is shown in Fig. 12, where $\lambda=1$ at 328 rpm, i.e., model 1 is suitable for the rotating speeds under 328 rpm. The amplitudes of the 1/rev responses are about 1000-3000 times the amplitudes of the 2/rev responses. The response in Figs. 12 has no significant differences from the responses of the uncracked system. However, the uncracked system does not possess 2/rev responses. Here the 2/rev responses are totally the crack messages. Resonance appears at the subcritical speeds (230, 1290, 4200, 4670 rpm), and the critical speeds(460, 2600 rpm) in the 2/rev response, Fig. 13. This is due to the fact that the equation of motion, with breathing model 1 for the crack, is nonlinear and the resonance at the critical speeds are excited by the coupling effects.

CONCLUSIONS

In this paper, the crack effects on vibration responses of the rotating shaft were represented by the crack released energy. The finite element approach was used to derive the stiffness reduction term, which can be added directly into the equation of motion for the cracked rotor-bearing system. Five possible crack breathing models were proposed, and model 1 (full crack area breathing) and model 4 (full crack area open) are the most frequent crack models used.

REFERENCE

Dimarogonas, A. D. & Paipetis, S. A., 1983, "Analytical Methods in Rotor Dynamics", Applied Science Puhlishers LTD., pp.145~148.

Gasch, R., 1976, "Dynamic Behavior of a Simple Rotor with a cross-sectional Crack", in Vibrations in Rotating Machinery, Institution of Mechanical Engineers, London, pp.123~128.

Grabowski, B., 1980, "The Vibrational Behavior of a Turbine Rotor Containing a Transverse Crack", ASME Journal of Mechanical Design, Vol 102, pp.140~146.

Mayes, I. W. and Davies, W. G. R., 1984, "Analysis of the Response of a Multi-Rotor-Bearing System Containing a Transverse Crack in a Rotor", ASME Journal of Vibration, Acoustics, Stress, and Reliability in Design, vol 106, pp.139~145.

Nelson, H. D. & Nataraj, C., 1986, "The Dynamics of a Rotator System with a Cracked Shaft", ASME Journal of Vibration, Acoustics, Stress, and Reliability in Design, vol 108, April, pp.189~196.

Nelson, H. D. & McVaugh, J. M., 1976, "The Dynamics of Rotator-Bearing Systems Using Finite Elements", ASME Journal of Engineering for Industry, May, pp.593~600.

Nelson, H. D., 1980, "A Finite Rotating Shaft Element Using Timoshenko Beam Theory", ASME Journal of Mechanical Design, vol. 102, October, pp. 793~803.

Papadopoulos, C. A. and Dimarogonas, A. D., 1988, "Coupled Longitudinal and Bending Vibration of a Cracked Shaft", ASME Journal of Vibration, Acoustics, Stress, and Reliability in Design, vol 110, Jan, pp.1~8.

Papadopoulos, C. A. and Dimarogonas, A. D., 1992, "Coupled Vibration of Cracked Shafts", ASME Journal of Vibration and Acoustics, vol 114, October, pp.461~467.

Tada. H., 1985, "The Stress Analysis of Cracks Handbook", 2nd edition, Del Research Corp., Hellertown, Pennsylvania.

Wauer, J., 1990, "On the Dynamics of Cracked Rotors : A Literature Survey", Apply Mechanics Review vol 43, no 1, Jan. pp.13~17.

shaft	Diameter mm	10
	Density kg/m**3	7860
	Young's Modulus Pa	2.0 e+11
	Poisson's Ratio	0.3
disk#1	Outer Dia. mm	80
	Inner Dia. mm	10
	Thickness mm	30
	Density kg/m**3	7860
	Eccentricity (x) mm	5.00
	Eccentricity (y) mm	2.00
disk#2	Outer Dia. mm	80
	Inner Dia. mm	10
	Thickness mm	20
	Density kg/m**3	7860
	Eccentricity (x) mm	2.00
	Eccentricity (y) mm	5.00
Bearings	stiffness matrix nt/m	1.0300 e8 6.8000 e6 -2.6000 e7 1.7658 e8
	damping matrix nt-sec/m	1.4000 e5 -1.2000 e3 -4.2000 e5 2.4000 e5

Table 1. Dimensions and properties of the rotor-bearing system

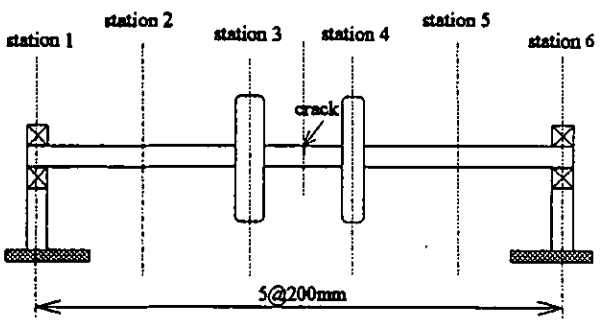

Figure 1. The rotor-bearing system with a mid-span crack

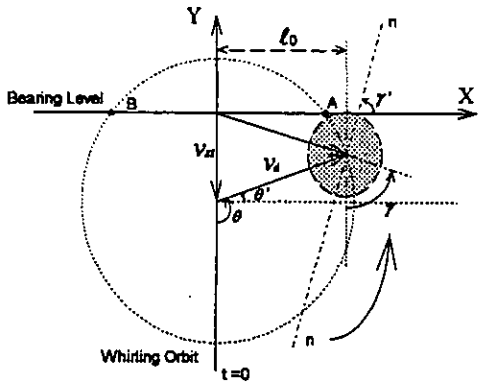

Figure 2. Deflections v_{st} and v_d, and the neutral axis of the shaft

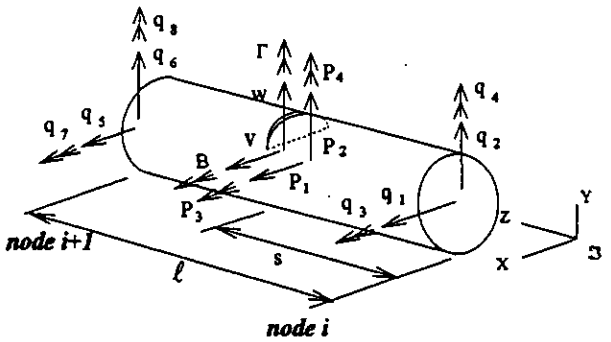

Figure 3.Generalized coordinates for FEM

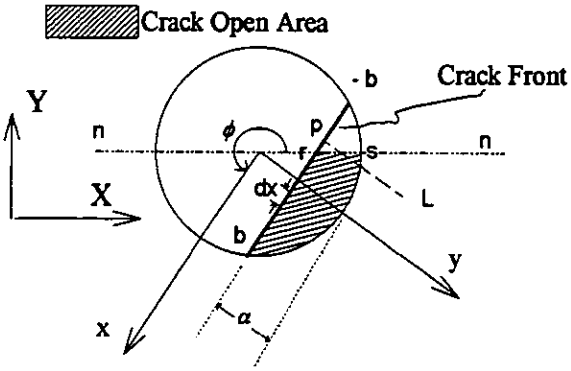

Figure 4. Integration area for the crack

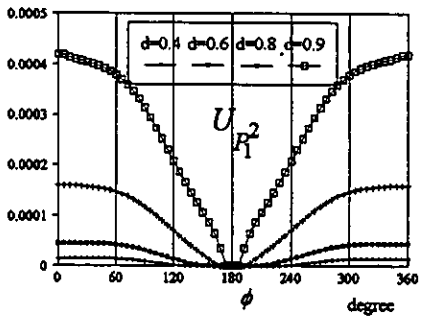

Figure 5. Crack released energy vs. rotating angle ϕ for P_1

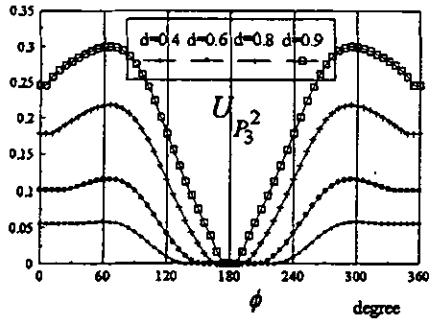

Figure 6. Crack released energy vs. rotating angle ϕ for P_3

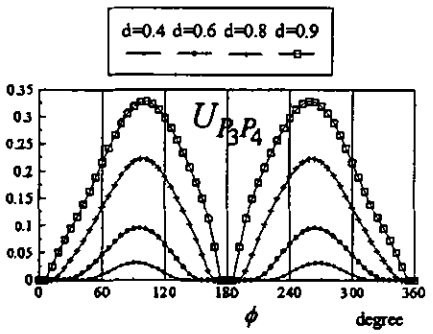

Figure 7. Crack released energy vs. rotating angle ϕ

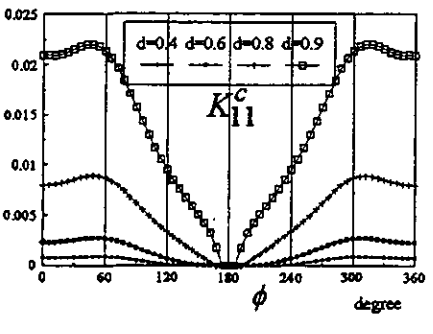

Figure 8. Stiffness reduction term K_{11}^c vs. rotating angle ϕ

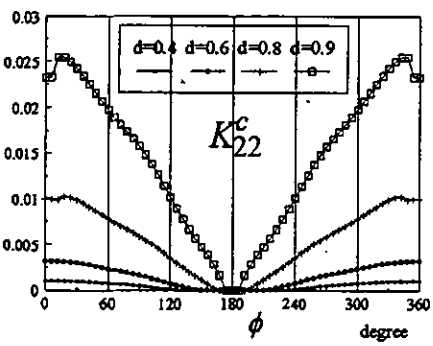

Figure 9. Stiffness reduction term K_{22}^c vs. rotating angle ϕ

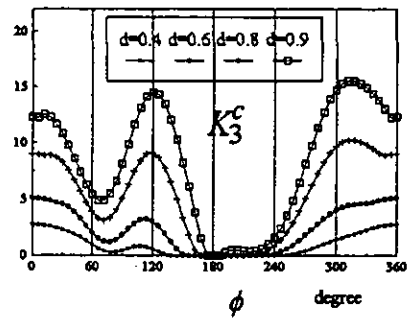

Figure 10. Stiffness reduction term K_{33}^c vs. rotating angle ϕ

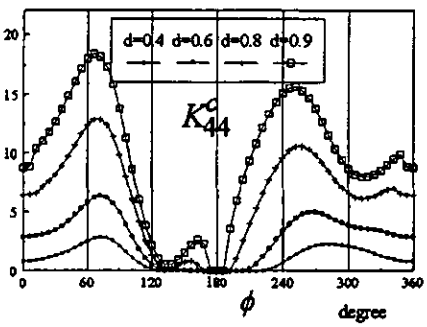

Figure 11. Stiffness reduction term K_{44}^c vs. rotating angle ϕ

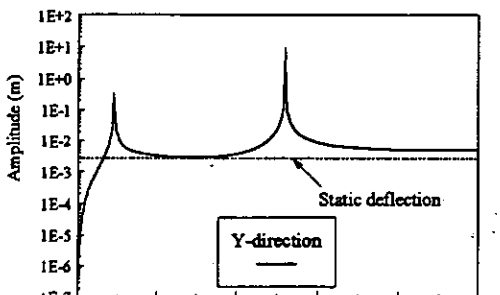

Figure 12. Amplitude response of the cracked system at station 2 (1/rev, $\alpha / R = 0.4$, model 1)

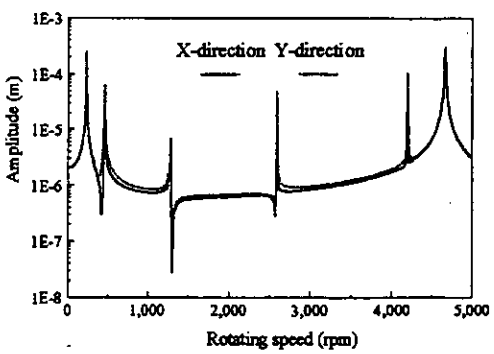

Figure 13. Amplitude response of the cracked system at station 2, (2/rev, $\alpha / R = 0.4$, model 1)